

Supporting information

Salt-Inclusion Chalcogenides with *d*-orbital Components: Unveiling Remarkable Nonlinear Optical Properties and Dual-Band Photoluminescence

Shao-Min Pei,^{a,b} Ming-Shu Zhang,^a Fan Wu,^{a,c} Yan Guo,^{a,c} Xiao-Ming Jiang,^{a,b} Bin-Wen Liu,^{*,a,b} Guo-Cong Guo^{*,a,b}

^a State Key Laboratory of Structural Chemistry, Fujian Institute of Research on the Structure of Matter, Chinese Academy of Sciences, Fuzhou, Fujian 350002, P. R. China.

^b Fujian Science & Technology Innovation Laboratory for Optoelectronic Information of China, Fuzhou, Fujian 350108, P. R. China.

^c College of Chemistry and Materials Science, Fujian Normal University, Fuzhou, Fujian, 350007, P. R. China.

1. Experimental Section

Syntheses

Polycrystalline $[K_4Cl][MnGa_9S_{12}]$ (**1**) and $[K_4Cl][HgGa_9S_{12}]$ (**2**) were synthesized through the conventional high-temperature solid-state reactions. The original reactant of La (31.2 mg, Macklin), Mn (12.4 mg, Aladdin), Ga (141.1 mg, Aladdin), S (115.3 mg, Xilong Scientific Co., Ltd.), and KCl (170 mg, Aladdin) were accurately weighed in a glovebox filled with argon to prepare crystal **1**. All the raw materials are procured commercially and utilized in their unprocessed state. The mixture was packed into a quartz tube, which was then sealed at an approximate pressure of 10^{-3} Torr. Subsequently, the tube was placed in a programmable furnace and subjected to the following firing process: it was gradually heated to 300 °C over a period of 6 h and maintained at this temperature for another 6 h, and then further heated to 600 °C over another 6 h period and held at this temperature for an additional 12 h. Subsequently, it was heated up to 900°C for 12 h and remained at this constant temperature for 96 h. The sample was eventually cooled down to 400 °C over a cooling time span of 96 hours. The synthesis process of crystal **2** was identical to that of **1**, with the exception that its synthetic raw materials was the mixtures of La (34.5 mg, Macklin), HgS (115.4 mg, Aladdin), Ga (86.5 mg, Aladdin), S (63.6 mg, Xilong Scientific Co., Ltd.), and KCl (170 mg, Aladdin). The reactants were heated to 300°C at room temperature for 6 hours, held at this temperature for 6 hours, then heated to 600°C for the same time, held at this temperature for 6 hours, and then heated to 950 °C for 12 hours, and cooled to room temperature for 4 days after being held at the highest temperature. The aggregated crystals were isolated subsequent to rinsing the products with deionized water in order to eliminate any remaining unreacted fluxing agent. The empirical molar ratios of K:Mn:Ga:S:Cl were determined to be 4.1:1.2:7.7:15.5:1 in **1**, and the molar ratios of K:Hg:Ga:S:Cl were measured to be 3.8:1:7.3:14.8:1 in **2**, which harmoniously aligned with their experimental formulas (Fig. S1).

Single Crystal and Powder X-ray Diffraction

The single-crystal X-ray diffraction (XRD) datasets of **1** and **2** were collected at 293 K on

a cutting-edge Rigaku FR-X microfocus diffractometer, which was equipped with a graphite monochromatic Mo- $K\alpha$ radiation source ($\lambda = 0.71073 \text{ \AA}$). The initial positions of all atoms were solved using direct methods, and the structures underwent refinement through the employment of the full matrix least squares technique F^2 , along with anisotropic thermal parameters for each atom. All calculations were executed utilizing the Siemens SHELXTL¹ version 5 crystallography software package.² Furthermore, to measure the powder XRD data of **1** (Fig. S2a) and **2** (Fig. S2b), we employed the Rigaku MiniFlex II X-ray diffractometer that boasted a diffractive monochromator specifically designed for Cu $K\alpha$ radiation ($\lambda = 1.54057 \text{ \AA}$). The purity of crystals **1** and **2** following irradiation with a 1910 nm laser at a power of 2 mJ for a duration of 30 minutes have been verified by XRD analysis. As shown in Fig. S3, the XRD curves of both **1** and **2** are consistent with the simulated curves, indicating that they still maintain good stability after laser experiments.

Infrared and UV–Vis–NIR Diffuse Reflectance Spectroscopy

The infrared spectra of **1** and **2** in microcrystalline forms were collected in the wavelength range of 4000–400cm⁻¹ was measured using a Nicolet Magana 750 FT-IR spectrophotometer. A base plate was prepared with BaSO₄ as a reference, and the sample was placed flat on its surface. Subsequently, the UV-Vis-NIR diffuse reflectance spectra of both compounds were recorded using a Perkin-Elmer Lambda 900 UV-Vis spectrophotometer within the wavelength range of 200–2500 nm. The reflectance spectra were then converted to an absorption spectrum utilizing the Kubelka-Munk formula: $F(R) = \alpha/S = (1-R)^2/2R$,³ where α represents the absorption coefficient, S denotes the scattering coefficient, and R signifies the reflectance. These data further underwent processing employing the Tauc plot formula $[F(R)\hbar v]^n = A(\hbar v - E_g)$, where n takes on a value of 2 for direct bandgap semiconductors and 0.5 for indirect bandgap semiconductors.

Second-Harmonic Generation (SHG) and Laser-Induced Damage Threshold (LIDT) Measurements

An improved Kurtz-Perry method⁴ was employed to assess the SHG responds of compounds **1** and **2** under the irradiation of 1910 nm laser. Microcrystalline samples with

particle sizes ranging from 30–50, 50–75, 75–100, 100–150, 150–200 μm , were screened for phase-matching measurements. AGS samples were acquired from a perfectly large-size crystal and sieved into same size ranges as a reference material. The frequency-doubled signals at a wavelength of 955 nm were detected using Andor's DU420A-BR-DD charge-coupled device (CCD) camera. The LIDTs of crystals **1–2** and the standard AGS were estimated via S-on-1 method, specifically, a high-power pulsed laser beam with wavelength of 2090 nm and pulse width (τ_p) of 10 ns was used to irradiate the single-crystals until damage to the surface was monitored. The damaged spot radius r was measured by Vernier calipers, and damage thresholds were calculated by using the equation $I_{(\text{threshold})} = E/(\pi r^2 \tau_p)$, where E represents the energy of single pulse.

Fluorescence Measurements

The photoluminescence spectrum of sample **1** was recorded on an Edinburgh FLS920 phosphorimeter using a 450W Xenon lamp as excitation source. The excitation wavelength was 470 nm, while the range of the emission wavelength was from 250 to 820 nm. Time-resolved spectra with long lifetime measurements were collected microsecond pulsed flash as the excitation. Temperature-dependent emission and decay data were collected using the FLS920 spectrophotometer equipped with a 10 K closed-cycle refrigeration cryogenic system at a series of temperature from 77 to 300 K. The Photoluminescence quantum efficiency (PLQE) measurement was conducted in the wavelength range of 490 to 820 nm using an Edinburgh FLS920. The fluorescence lifetime is fitted by a triple exponential function:

$$F(t) = A_1 \exp(-t/\tau_1) + A_2 \exp(-t/\tau_2) + A_3 \exp(-t/\tau_3)$$

Where A_1 , A_2 , A_3 represent the amplitude of the triple exponential function, and τ_1 , τ_2 , τ_3 represent the time constant of the triple exponential function.

Computation Procedure

The electronic band structure of **1** and **2** were computationally determined using the CASTEP module within Materials Studio package, which is based on density functional

theory (DFT)⁵. For the exchange-correlation functional, we selected the Perdew, Burke, and Ernzerhof (PBE) parametrized generalized Generalized gradient approximation (GGA)⁶. Valence configurations K- $3s^23p^64s^1$, Mn- $3p^63d^54s^2$, Hg- $5d^{10}6s^2$, Ga- $3d^{10}4s^24p^1$, S- $3s^23p^4$, and Cl- $3s^23p^5$ were used with projector-augmented plane-wave pseudopotentials, and the plane-wave energy cut-off was set at 18 Hartree. To perform numerical integration of the Brillouin zone, a Monkhorst–Pack κ -point mesh with dimensions of $4 \times 4 \times 4$ was utilized. The linear and nonlinear optical properties of compound **1** and **2** were performed using the *ABINIT* package based on DFT.⁷⁻¹¹ The complex dielectric function $\varepsilon_{ij,re} = \varepsilon_{ij,re}(\omega) + \varepsilon_{ij,im}(\omega)$ were calculated using
$$\frac{4\pi}{\Omega} \sum_{nmk} f_{nm}(k) \frac{r_{nm}^i(k) r_{mn}^j(k)}{\omega_{mn}(k) - \omega} + \delta_{ij}$$
 to describe the linear optical properties of **1** and **2**, where $\varepsilon_{re}(\omega)$ represents real part while $\varepsilon_{im}(\omega)$ represents imaginary part of the dielectric function, respectively. Position matrix elements $r_{nm}^i(k)$ between states n and m were also considered in this calculation. Furthermore, frequency-dependent SHG susceptibility tensors $\chi_{ijk}(2\omega, \omega, \omega)$ were evaluated by employing DFT and “sum over states” method. It should be noted that the SHG susceptibility consists of three components: pure interband transition term $\chi_{\text{inter}}(2\omega, \omega, \omega)$, intraband transition term $\chi_{\text{intra}}(2\omega, \omega, \omega)$ describing the modulation of linear susceptibility by the intraband motion of the electron, as well as modulation term denoted as $\chi_{\text{mod}}(2\omega, \omega, \omega)$ accounting for intraband contribution influenced by motion-related polarization energy.¹¹ The angular average SHG susceptibility tensor square $\langle d_{ijk}^2 \rangle$ ¹² was calculated based on the following formulas :

$$\langle d^2 \rangle = \frac{19}{105} \sum_i d_{iii}^2 + \frac{13}{105} \sum_{i \neq j} d_{iii} d_{ijj} + \frac{44}{105} \sum_{i \neq j} d_{ijj}^2 + \frac{13}{105} \sum_{ijk, \text{cyclic}} d_{iij} d_{jkk} + \frac{5}{7} d_{ijk}^2.$$

The atomic-resolved SHG susceptibility tensors were obtained by aggregating contributions from all orbitals attributed to the target atoms. The specific calculation formulas of atom-resolved SHG contributions are provided below:

$$\varphi = C_1 \varphi_{Ga-s} + C_2 \varphi_{Ga-p} + \dots$$

$$W_i = \frac{|C_i|^2}{\sum |C_i|^2}$$

$$\chi_{orbital} = W_i \chi_{energy level}$$

$$\chi_{atom} = \sum \chi_{orbital}$$

$$\chi_{element} = \sum_{atom \text{ in cell}} \chi_{atom}$$

Where C_i represents the coefficient of orbital composition, φ represents the wave function of energy level, and χ represents SHG coefficient.

2. Figures and Tables

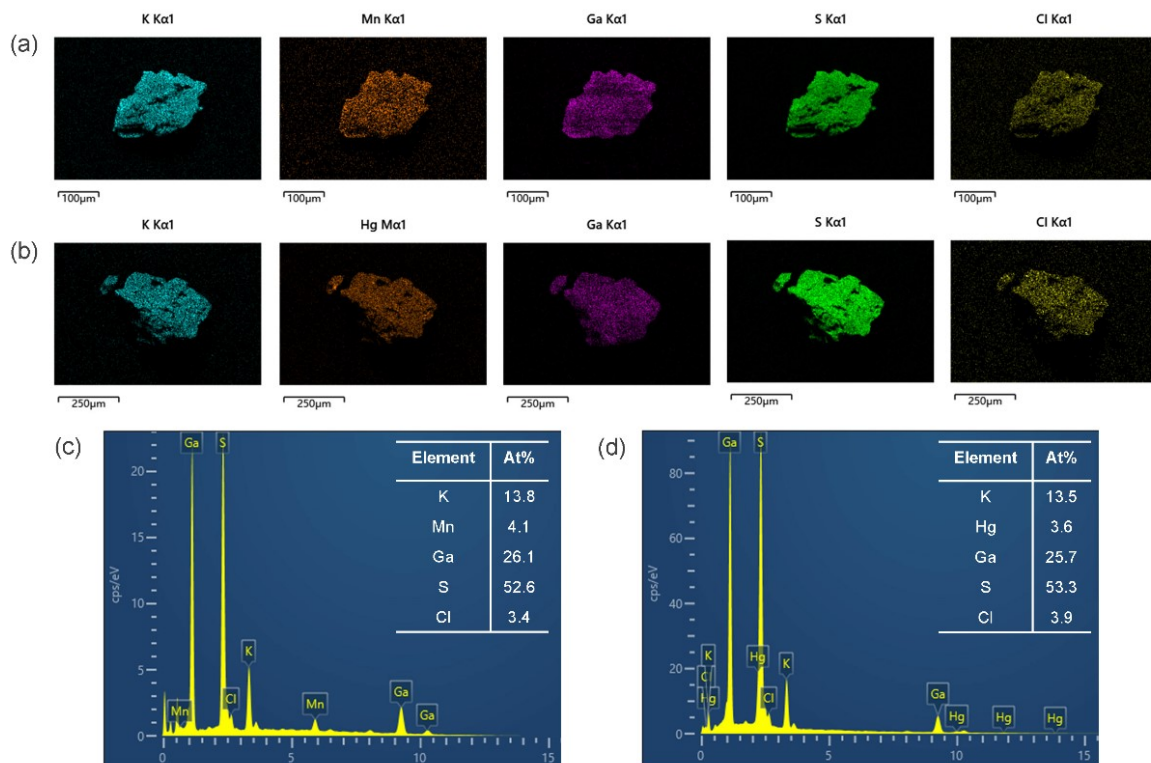


Figure S1. The SEM images and EDS mapping analyses of **1** (a, c) and **2** (b, d).

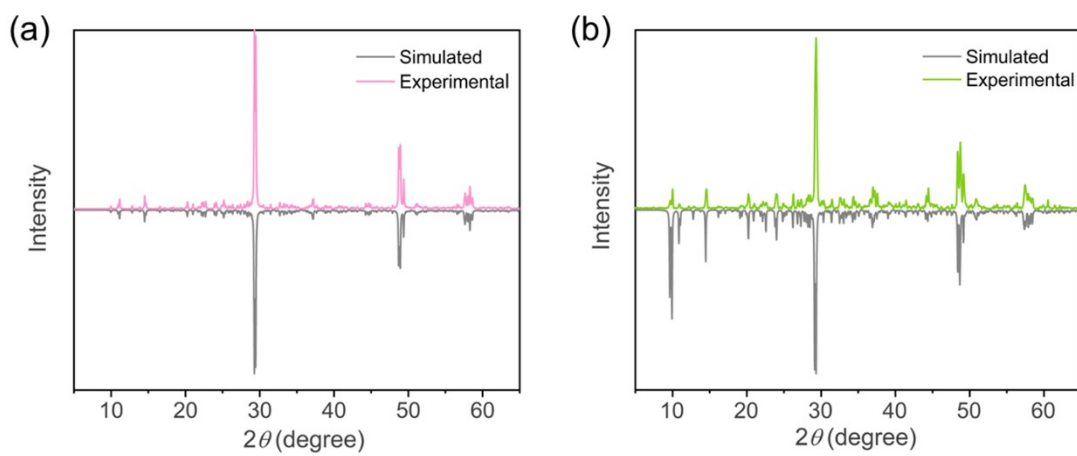


Figure S2. The experimental and simulated powder XRD patterns of **1** (a) and **2** (b).

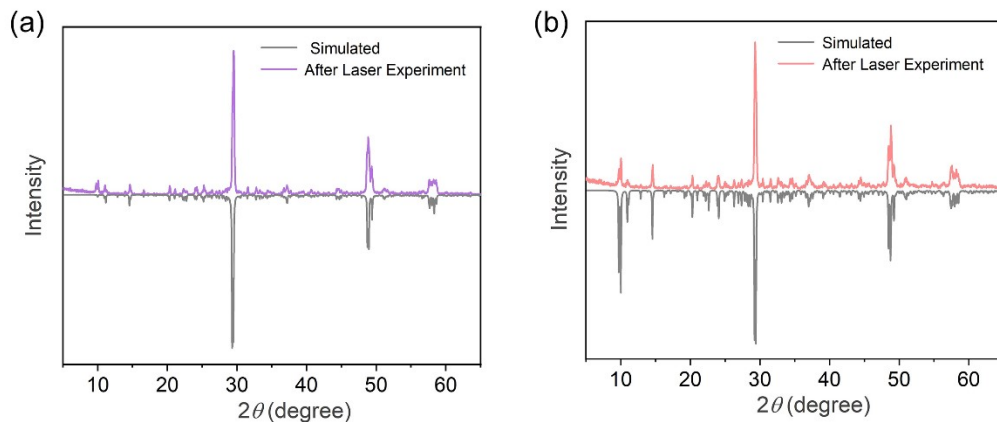


Figure S3. The XRD curves of compounds **1** (a) and **2** (b) after laser experiments.

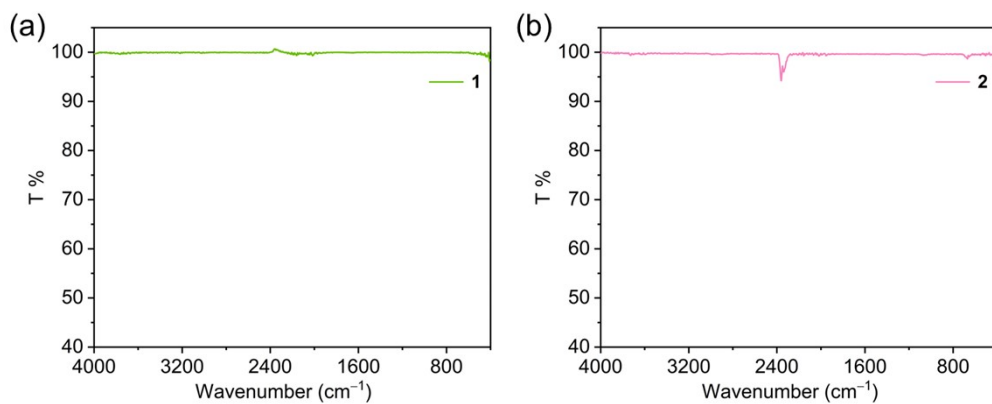


Figure S4. The infrared spectra of **1** (a) and **2** (b).

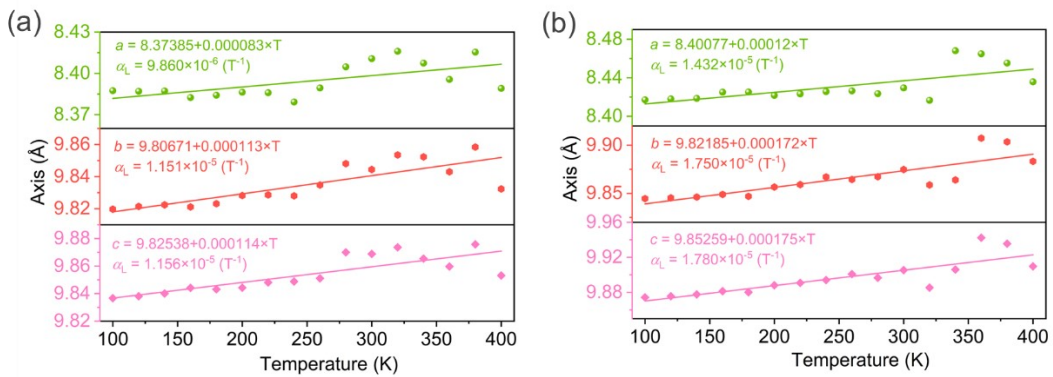


Figure S5. Variable-temperature lattice parameters of *a*-, *b*-, and *c*-axes in **1** (a) and **2** (b).

Table S1. Crystallographic data and structure refinement parameters for **1** and **2**.

Empirical formula	[K ₄ Cl][MnGa ₉ S ₁₆] (1)	[K ₄ Cl][HgGa ₉ S ₁₆] (2)
CCDC	2326388	2326389
<i>F</i> _w	1387.23	1532.88
Temperature (K)	293(2)	293(2)
Space group	<i>P</i> 1	<i>P</i> 1
<i>a</i> (Å)	8.4110(5)	8.4316(3)
<i>b</i> (Å)	9.8534(7)	9.8787(4)
<i>c</i> (Å)	9.8840(11)	9.8986(4)
<i>V</i> (Å ³)	735.54(12)	739.08(5)
<i>α</i> (Å ³)	68.488(9)	68.220(4)
<i>β</i> (Å ³)	74.848(7)	74.878(3)
<i>γ</i> (Å ³)	85.152(5)	84.986(3)
<i>Z</i>	1	1
<i>D</i> _{calcd} (g·cm ⁻³)	3.132	3.444
<i>μ</i> (mm ⁻¹)	10.307	15.017
<i>GOF</i> on <i>F</i> ²	1.002	1.000
<i>R</i> ₁ ^a (<i>I</i> > 2σ(<i>I</i>))	0.0373	0.0486
<i>wR</i> ₂ ^b (<i>I</i> > 2σ(<i>I</i>))	0.0905	0.1129
<i>R</i> ₁ ^a (all data)	0.0396	0.0541

wR_2^b (all data)	0.0915	0.1154
$\Delta\rho_{\text{max}}/\Delta\rho_{\text{min}}$ (e Å ⁻³)	2.67/-0.87	4.87/-1.66

^a $R = \sum |F_o| - |F_c| | / \sum |F_o|$, ^b $wR = (\sum (w(F_o^2 - F_c^2)^2) / \sum (w(F_o^2)^2))^{1/2}$.

Table S2. Coordinates ($\times 10^4$) and equivalent isotropic displacement parameters (Å² $\times 10^3$) of all crystallographically independent atoms in **1** and **2**.

Atoms	x	y	z	$U^{(\text{eq})}$
1				
K1	1380(4)	1327(3)	4012(3)	34.5(7)
K2	10003(4)	9989(3)	10015(4)	37.3(7)
K3	7892(4)	4306(4)	928(4)	45.3(8)
K4	3706(4)	3574(3)	9278(4)	39.8(8)
Cl1	540(4)	2208(4)	1168(4)	31.7(7)
Mn1	2867(2)	6984(2)	5455(2)	16.3(4)
Ga1	9860.0(15)	3974.2(12)	6431.3(15)	12.6(3)
Ga2	4015.0(15)	7932.1(12)	8508.5(14)	13.1(3)
Ga3	8257.6(17)	7532.1(15)	6922.3(18)	15.2(3)
Ga4	5846.5(17)	9977.1(16)	4378.5(18)	12.6(3)
Ga5	7376.6(16)	6538.3(13)	3839.8(15)	15.5(3)
Ga6	7029.2(16)	982.7(14)	7313.5(15)	13.8(3)
Ga7	4253.8(15)	3551.1(14)	4883.7(16)	14.6(4)
Ga8	2075.5(15)	6030.3(13)	2318.3(14)	13.3(3)
Ga9	5069.4(15)	8933.7(14)	1477.4(16)	14.3(3)
S1	7591(4)	2745(3)	8060(3)	15.5(6)
S2	5128(3)	5282(3)	5595(3)	15.4(6)
S3	9560(3)	4912(3)	3953(3)	13.3(6)
S4	4584(3)	9939(3)	9054(3)	12.9(6)
S5	5426(4)	887(3)	2062(3)	19.7(7)
S6	3509(4)	8951(3)	6139(3)	14.4(6)
S7	6502(4)	1938(3)	4914(3)	13.1(6)

S8	6024(4)	6315(3)	8531(4)	19.3(6)
S9	8089(3)	8450(3)	4417(3)	13.9(6)
S10	314(3)	5832(3)	7175(3)	15.8(6)
S11	7206(4)	7400(3)	1465(4)	19.1(6)
S12	2498(4)	7997(3)	2916(3)	16.4(6)
S13	2015(4)	2466(3)	6677(4)	18.6(7)
S14	1626(4)	6835(3)	10006(3)	16.4(6)
S15	9147(3)	9460(3)	7219(4)	18.8(6)
S16	3941(4)	4244(3)	2546(3)	18.4(6)
2				
K1	1366(7)	1339(5)	4020(6)	39.9(13)
K2	10001(7)	9988(5)	9993(6)	42.1(13)
K3	7880(8)	4304(6)	951(6)	49.9(15)
K4	3678(7)	3580(6)	9275(6)	45.2(14)
Cl1	526(8)	2200(6)	1168(7)	34.5(12)
Hg1	2846.6(9)	6988.6(7)	5476.6(8)	24.2(3)
Ga1	9849(4)	3968(3)	6432(3)	13.4(5)
Ga2	3997(3)	7949(3)	8510(3)	14.1(5)
Ga3	8219(3)	7519(3)	6932(3)	14.3(5)
Ga4	5848(3)	9988(2)	4378(2)	14.1(6)
Ga5	7383(3)	6530(2)	3841(3)	16.4(5)
Ga6	7028(3)	975(2)	7310(2)	10.9(5)
Ga7	4260(3)	3551(2)	4886(3)	17.4(5)
Ga8	2072(3)	6043(2)	2300(2)	15.9(6)
Ga9	5045(3)	8947(2)	1475(3)	14.2(5)
S1	7597(7)	2715(5)	8064(6)	18.5(11)
S2	5212(6)	5212(5)	5632(6)	19.1(11)
S3	9577(6)	4922(5)	3951(5)	15.0(10)
S4	4581(6)	9947(5)	9049(5)	15.6(10)

S5	5387(7)	881(5)	2084(6)	22.1(12)
S6	3496(6)	9056(5)	6154(5)	15.2(10)
S7	6518(6)	1953(5)	4885(5)	13.3(10)
S8	5981(6)	6307(5)	8546(6)	19.2(11)
S9	8066(6)	8437(5)	4424(5)	15.3(10)
S10	223(6)	5777(5)	7260(5)	18.4(11)
S11	7194(7)	7411(6)	1477(6)	23.1(11)
S12	2453(6)	8050(5)	2829(5)	18.1(11)
S13	2027(7)	2482(5)	6676(6)	21.0(11)
S14	1629(7)	6838(5)	9998(6)	17.8(10)
S15	9136(7)	9433(5)	7221(6)	22.6(11)
S16	3944(7)	4260(6)	2550(6)	21.4(11)

Table S3. Selected bond lengths [Å] for **1** and **2**.

Bonds	Distances	Bonds	Distances	Bonds	Distances
1					
K1-Cl1	2.880(5)	Ga2-S14	2.244(3)	Ga6-S7	2.356(3)
K2-Cl1	2.923(5)	Ga3-S8	2.217(3)	Ga6-S15	2.235(3)
K3-Cl1	2.903(4)	Ga3-S9	2.343(3)	Ga7-S2	2.303(3)
K4-Cl1	2.925(4)	Ga3-S10	2.300(3)	Ga7-S7	2.364(3)
Mn1-S2	2.424(3)	Ga3-S15	2.240(3)	Ga7-S13	2.244(3)
Mn1-S6	2.416(3)	Ga4-S5	2.244(3)	Ga7-S16	2.238(3)
Mn1-S10	2.424(4)	Ga4-S6	2.275(3)	Ga8-S3	2.367(3)
Mn1-S12	2.430(4)	Ga4-S7	2.323(3)	Ga8-S12	2.301(3)
Ga1-S1	2.248(3)	Ga4-S9	2.311(3)	Ga8-S14	2.251(3)
Ga1-S3	2.354(3)	Ga5-S2	2.285(3)	Ga8-S16	2.244(3)
Ga1-S10	2.300(3)	Ga5-S3	2.331(3)	Ga9-S4	2.364(3)
Ga1-S13	2.250(3)	Ga5-S9	2.321(3)	Ga9-S5	2.265(3)
Ga2-S6	2.323(3)	Ga5-S11	2.224(3)	Ga9-S11	2.249(3)

Ga2-S8	2.221(3)	Ga6-S1	2.245(3)	Ga9-S12	2.306(3)
Ga2-S4	2.346(3)	Ga6-S4	2.336(3)		
2					
K1-Cl1	2.889(7)	Ga2-S14	2.238(6)	Ga6-S7	2.371(5)
K2-Cl1	2.941(7)	Ga3-S8	2.225(6)	Ga6-S15	2.243(5)
K3-Cl1	2.907(7)	Ga3-S9	2.341(5)	Ga7-S2	2.306(5)
K4-Cl1	2.928(8)	Ga3-S10	2.298(5)	Ga7-S7	2.365(5)
Hg1-S2	2.536(5)	Ga3-S15	2.242(5)	Ga7-S13	2.240(6)
Hg1-S6	2.515(4)	Ga4-S5	2.235(5)	Ga7-S16	2.235(6)
Hg1-S10	2.510(5)	Ga4-S6	2.274(5)	Ga8-S3	2.365(6)
Hg1-S12	2.536(5)	Ga4-S7	2.324(4)	Ga8-S12	2.298(5)
Ga1-S1	2.252(6)	Ga4-S9	2.311(5)	Ga8-S14	2.239(5)
Ga1-S3	2.347(5)	Ga5-S2	2.280(6)	Ga8-S16	2.246(5)
Ga1-S10	2.299(5)	Ga5-S3	2.328(6)	Ga9-S4	2.357(5)
Ga1-S13	2.254(6)	Ga5-S9	2.321(5)	Ga9-S5	2.267(5)
Ga2-S6	2.314(5)	Ga5-S11	2.218(6)	Ga9-S11	2.259(5)
Ga2-S8	2.224(5)	Ga6-S1	2.242(5)	Ga9-S12	2.299(6)
Ga2-S4	2.348(5)	Ga6-S4	2.338(5)		

Table S4. The laser-induced damage thresholds of **1**, **2**, and AgGaS₂ determined by single crystals.

Compounds	Damage energy (mJ)	Spot area (cm ²)	τ _p (ns)	Damage threshold ^a [MW·cm ⁻²]
1	4.2	0.020	10	20.8
2	4.3	0.020	10	21.3
AgGaS ₂	0.8	0.020	10	4.0

^a Both **1** and **2** was measured by three times with different single crystals.

Table S5. Summary of Hg-based NLO chalcogenides.

Compounds	SHG (×AGS)	E _g (eV)	PM/NPM ^a
-----------	------------	---------------------	---------------------

HgCuPS ₄ ¹³	6.5	2.03	PM
Na ₂ Hg ₃ Sn ₂ S ₈ ¹⁴	2.8	2.45	PM
AgHgPS ₄ ¹⁵	5.09	2.63	PM
Na ₂ Hg ₃ Ge ₂ S ₈ ¹⁴	2.2	2.68	PM
δ -K ₂ Hg ₃ Ge ₂ S ₈ ¹⁶	1.5	2.70	PM
SrHgSnS ₄ ¹⁷	1.9	2.72	PM
BaHgSnS ₄ ¹⁷	2.8	2.77	PM
Hg ₃ P ₂ S ₈ ¹⁸	4.2	2.77	PM
HgGa ₂ S ₄ ¹⁹	2.3	2.81	PM
Na ₂ Hg ₃ Si ₂ S ₈ ¹⁴	1.3	2.86	PM
BaHgSiS ₄ ²⁰	2.1	2.94	PM
[Ba ₄ Cl ₂][HgGa ₄ S ₁₀] ²¹	1.1	2.95	PM
SrHgGeS ₄ ²⁰	2.4	2.97	PM
BaHgGeS ₄ ²⁰	1.8	3	PM
SrHgSiS ₄ ²⁰	2	3.06	PM
Zn ₂ HgP ₂ S ₈ ²²	2.2	3.37	PM
BaHgS ₂ ²³	6.5	1.93	NPM
BaHgSe ₂ ²⁴	1.5	1.56	\
Hg ₂ GeSe ₄ ²⁵	2.1	1.17	PM
Na ₂ Hg ₃ Si ₂ Se ₈ ²⁶	3.6	2.20	PM
Na ₂ Hg ₃ Ge ₂ Se ₈ ²⁶	4.8	1.98	PM
Na ₂ Hg ₃ Sn ₂ Se ₈ ²⁶	5.4	1.88	PM
Li ₂ HgSiS ₄ ²⁷	0.8	2.68	NPM
Li ₂ HgGeS ₄ ²⁷	3.0	2.46	NPM
Li ₂ HgSnS ₄ ²⁷	4.0	2.32	NPM
Li ₂ HgGeSe ₄ ²⁶	4.6	2.27	PM
Li ₂ HgSnSe ₄ ²⁶	6.0	1.93	PM
Li ₄ HgSn ₂ Se ₇ ²⁸	3.6	2.10	PM
Li ₄ HgGe ₂ S ₇ ²⁹	1.5	2.75	\

Compounds	SHG (×AGS)	E _g (eV)	Compounds	SHG (×AGS)	E _g (eV)
BaHgGeSe ₄ ³⁰	4.7	2.49	PM		
SrHgGeSe ₄ ³⁰	4.8	2.42	PM		
BaHgSnSe ₄ ¹⁷	5.1	1.98	PM		
SrHgSnSe ₄ ¹⁷	4.9	2.07	PM		
EuHgGeS ₄ ³¹	0.9	2.04	PM		
EuHgGeSe ₄ ³²	1.77	2.14	PM		
EuHgSnS ₄ ³²	3.1	1.97	PM		
Ag ₆ HgGeSe ₆ ³³	0.5	0.92	PM		
Ag ₆ HgSiSe ₆ ³³	2.0	1.0	PM		
KHg ₄ Ga ₅ Se ₁₂ ³⁴	20	1.61	PM		
RbHg ₄ Ga ₅ S ₁₂ ³⁵	1.1	2.30	NPM		
CsHg ₄ Ga ₅ S ₁₂ ³⁵	1.8	2.36	NPM		
Hg ₇ P ₂ Se ₁₂ ³⁶	1	1.40	PM		
Hg ₃ AsS ₄ Cl ³⁷	2.8	2.41	PM		
Hg ₃ AsS ₄ Cl ³⁷	3.2	2.43	PM		
Hg ₃ AsSe ₄ Br ³⁸	8.8	2.13	PM		
Hg ₃ AsSe ₄ I ³⁸	6.2	2.10	PM		
CsClHg ₃ P ₂ S ₈ ³⁹	0.8	3.0	PM		
CsBrHg ₃ P ₂ S ₈ ³⁹	1.2	2.95	PM		
RbBrHg ₃ P ₂ S ₈ ³⁹	1.05	2.94	PM		
HgS ⁴⁰	1.2	2.04	PM		
[K ₄ Cl][HgGa ₉ S ₁₆] ^{this work}	1.0	3.41	PM		

^a Phase-matching (PM) and nonphase-matching (NPM) behavior.

Table S6. A brief summary of phase-matching behavior SIC NLO materials and their SHG intensities and band gaps.

Compounds	SHG (×AGS)	E _g (eV)	Compounds	SHG (×AGS)	E _g (eV)
[Sr ₄ Cl ₂][Si ₃ S ₉] ⁴¹	1.2	4.22	[K ₂ PbI][Ga ₇ S ₁₂] ⁴⁸	2.7	2.41
[K ₃ Cl][Ga ₃ PS ₈] ⁴²	1.00	3.60	[Na ₂ PbI][Ga ₇ S ₁₂] ⁴⁹	2.6	2.53

[Rb ₃ Cl][Ga ₃ PS ₈] ⁴²	1.10	3.65	[K ₄ Cl][CdGa ₉ S ₁₆] ⁵⁰	0.9	3.15
[K ₃ Br][Ga ₃ PS ₈] ⁴²	1.20	3.85	[K ₄ Cl][CdGa ₉ Se ₁₆] ⁵⁰	2.4	1.72
[Rb ₃ Br][Ga ₃ PS ₈] ⁴²	2.00	3.50	[K ₃ Cl][Mn ₂ Ga ₆ S ₁₂] ⁵¹	0.8	3.17
[RbBa ₂ Cl][Ga ₄ S ₈] ⁴³	1.00	3.30	Rb ₆ [K ₃ Cl][Li ₂ Mn ₄ Ga ₁₂ S ₂₇] ⁵²	1.1	3.31
[CsBa ₂ Cl][Ga ₄ S ₈] ⁴³	0.90	3.35	[CsBa ₃ Br][B ₂ S ₆] ⁵³	0.5	2.65
Li[LiCs ₂ Cl][Ga ₃ S ₆] ⁴⁴	0.70	4.18	[CsBa ₃ I][B ₂ S ₆] ⁵³	0.5	2.71
[Ba ₄ Cl ₂][ZnGa ₄ S ₁₀] ⁴⁵	1.1	3.85	[RbBa ₃ Br][B ₂ S ₆] ⁵³	0.6	2.61
[Ba ₄ Cl ₂][HgGa ₄ S ₁₀] ⁴⁶	1.5	2.95	[RbBa ₃ I][B ₂ S ₆] ⁵³	0.5	2.64
[KBa ₃ Cl ₂][Ga ₅ S ₁₀] ⁴⁷	1.0	3.93	[RbBa ₃ Cl][In ₈ Se ₁₄] ⁵⁴	2	2.02
[RbBa ₃ Cl ₂][Ga ₅ S ₁₀] ⁴⁷	1.0	3.95	[Na ₄ I][Ga ₉ S ₁₅] ⁵⁵	0.7	3.10
[CsBa ₃ Cl ₂][Ga ₅ S ₁₀] ⁴⁷	1.0	3.96	[K ₄ Cl][MnGa ₉ S ₁₆] (this work)	0.6	3.02
[K ₂ PbCl][Ga ₇ S ₁₂] ⁴⁸	2.5	2.54	[K ₄ Cl][HgGa ₉ S ₁₆] (this work)	1.0	3.41
[K ₂ PbBr][Ga ₇ S ₁₂] ⁴⁸	2.6	2.49			

3. References

1. G. M. Sheldrick, University of Gö ttingen: Gö ttingen, Germany, 1997.
2. Rigaku Oxford Diffraction, CrysAlisPro Software System, Version v40.67a, Rigaku Corporation, Oxford, UK, 2019.
3. G. Korum, *Springer: New York*, 1969.
4. D. J. Clark, J.-H. Zhang, A. J. Craig, A. Weiland, J. A. Brant, J. B. Cho, Y. S. Kim, J. I. Jang, and J. A. Aitken, The Kurtz-Perry Powder Technique Revisited: A Case Study on the Importance of Reference Quality and Broadband Nonlinear Optical Measurements Using LiInSe₂. *J. Alloys Compd.*, 2022, **917**, 165381.
5. S. J. Clark, M. D. Segall, C. J. Pickard, P. J. Hasnip, M. J. Probert, K. Z. Refson, and M. C. Payne, First Principles Methods Using CASTEP. *Z. Kristallogr. Cryst. Mater.*, 2005, **220**, 567–570.
6. J. P. Perdew, J. A. Chevary, S. H. Vosko, K. A. Jackson, M. R. Pederson, D. J. Singh, and C. Fiolhais, Atoms, Molecules, Solids, and Surfaces: Applications of the Generalized Gradient Approximation for Exchange and Correlation. *Phys. Rev. B*, 1992, **46**, 6671–6687.
7. X. Gonze, *Phys. Rev. A*, 1995, **52**, 1086–1095.
8. X. Gonze, *Phys. Rev. A*, 1995, **52**, 1096–1114.

9. P. Ghosez, X. Gonze, and R. W. Godby., *Phys. Rev. B*, 1997, **56**, 12811–12817.
10. S. Baroni, S. Gironcoli, A. D. Corso, and P. Giannozzi, *Rev. Mod. Phys.*, 2001, **73**, 515–562.
11. S. Sharma, and C. A. Draxl, *Phys. Scr.*, 2004, **T109**, 128–134.
12. S. K. Kurtz, and T. T. Perry, *J. Appl. Phys.*, 1968, **39**, 3798–3813.
13. M. Li, Z. Ma, B. Li, X. Wu, H. Lin, and Q. Zhu, *Chem. Mater.*, 2020, **32**, 4331–4339.
14. K. Wu, Z. Yang, and S. Pan, *Chem. Mater.*, 2016, **28**, 2795–2801.
15. W. Xing, N. Wang, C. Tang, C. Li, Z. Lin, J. Yao, W. Yin, and B. Kang, *J. Mater. Chem. C*, 2021, **9**, 1062–1068.
16. J. Liao, G. Marking, K. Hsu, Y. Matsushita, M. Ewbank, R. Borwick, P. Cunningham, M. Rosker, and M. Kanatzidis, *J. Am. Chem. Soc.*, 2003, **125**, 9484–9493.
17. Y. Guo, F. Liang, Z. Li, W. Xing, Z. Lin, J. Yao, A. Mar, and Y. Wu, *Inorg. Chem.*, 2019, **58**, 10390–10398.
18. Y. Chu, H. Wang, T. Abutukadi, Z. Li, M. Mutailipu, X. Su, Z. Yang, J. Li, and S. Pan, *Small*, 2023, **19**, 2305074.
19. N. Umemura, T. Mikami, and K. Kato, *Opt. Commun.*, 2012, **285**, 1394–1396.
20. X. Zhang, H. Wu, Z. Hu, J. Wang, Y. Wu, and H. Yu, *Adv. Opt. Mater.*, 2023, 2301735.
21. Y. Zhang, H. Wu, Z. Hu, J. Wang, Y. Wu, and H. Yu, *Inorg. Chem. Front.*, 2022, **9**, 4075–4080.
22. Y. Chu, H. Wang, T. Abutukadi, Z. Li, M. Mutailipu, X. Su, Z. Yang, J. Li, and S. Pan, *Small*, 2023, **19**, 2305074.
23. K. Wu, X. Su, and S. Pan, Z. Yang, *Inorg. Chem.*, 2015, **54**, 2772–2779.
24. C. Li, W. Yin, P. Gong, X. Li, M. Zhou, A. Mar, Z. Lin, J. Yao, Y. Wu, and C. Chen, *J. Am. Chem. Soc.*, 2016, **138**, 6135–6138.
25. Y. Guo, F. Liang, J. Yao, Z. Lin, W. Yin, Y. Wu, and C. Chen, *Inorg. Chem.*, 2018, **57**, 6795–6798.
26. L. Gao, J. Xu, X. Tian, B. Zhang, X. Wu, and K. Wu, *Chem. Mater.*, 2022, **34**, 5991–5998.
27. K. Wu, S. Pan, *Crystals*, 2017, **7**, 107.
28. Y. Guo, F. Liang, Z. Li, W. Xing, Z. Lin, J. Yao, and Y. Wu, *Cryst. Growth Des.*, 2019, **19**, 5494–5497.
29. K. Wu, Z. Yang, and S. Pan, *Chem. Commun.*, 2017, **53**, 3010–3013.

30. Y. Guo, F. Liang, W. Yin, Z. Li, X. Luo, Z. Lin, J. Yao, A. Mar, and Y. Wu, *Chem. Mater.*, 2019, **31**, 3034–3040.
31. M. Yan, Z.-D. Sun, W.-D. Yao, W. Zhou, W. Liu, and S.-P. Guo, *Inorg. Chem. Front.*, 2020, **7**, 2451–2458.
32. W. Xing, C. Tang, N. Wang, C. Li, Z. Li, J. Wu, Z. Lin, J. Yao, W. Yin, and B. Kang, *Inorg. Chem.*, 2020, **59**, 18452–18460.
33. L. D. Gulay, I. D. Olekseyuk, and O. V. Parasyuk, *J. Alloys Compd.*, 2002, **343**, 116–121.
34. M. Zhou, Y. Yan, Y. Guo, Z. Lin, J. Yao, Y. Wu, and C. Chen, *Chem. Mater.*, 2017, **29**, 7993–8002.
35. X. Lou, Y. Zhou, W.-F. Chen, X.-M. Jiang, B.-W. Liu, and G.-C. Guo, *Dalton Trans.*, 2023, **52**, 4873–4879.
36. Y. Chu, H. Wang, Q. Chen, X. Su, Z. Chen, Z. Yang, J. Li, and S. Pan, *Adv. Funct. Mater.*, 2023, 2314933.
37. F. Xu, X. Xu, B. Li, G. Zhang, C. Zheng, J. Chen, and N. Ye, *Inorg. Chem. Front.*, 2024, DOI: 10.1039/D4QI00032C.
38. J. Chen, C. Lin, X. Jiang, G. Yang, M. Luo, X. Zhao, B. Li, G. Peng, N. Ye, Z. Hu, J. Wang, and Y. Wu, *Mater. Horiz.*, 2023, **10**, 2876–2882.
39. W. Xing, C. Tang, N. Wang, C. Li, E. Uykur, J. Wu, Z. Lin, J. Yao, W. Yin, and B. Kang, *Adv. Optical Mater.*, 2021, **9**, 2100563.
40. M. Yan, W.-D. Yao, W.-L Liu, R.-L. Tang, and S.-P. Guo, Helical. *Inorg. Chem.*, 2021, **60**, 16917–16921.
41. C. Zhao, K. Wu, Y. Xiao, B. Zhang, H. Yu, H. Zhang, *J. Mater. Chem. C*, 2023, **11**, 4439–4443.
42. B.-W. Liu, H.-Y. Zeng, X.-M. Jiang, G.-E. Wang, S.-F. Li, L. Xu, G.-C. Guo, *Chem. Sci.*, 2016, **7**, 6273.
43. B.-W. Liu, X.-M. Jiang, H.-Y. Zeng, and G.-C. Guo, *J. Am. Chem. Soc.*, 2020, **142**, 10641–10645.
44. B.-W. Liu, X.-M. Jiang, B.-X. Li, H.-Y. Zeng, and G.-C. Guo, *Angew. Chem. Int. Ed.*, 2020, **59**, 4856–4859.
45. H. Chen, Y. Li, B. Li, P. Liu, H. Lin, Q. Zhu, and X. Wu, *Chem. Mater.*, 2020, **32**, 8012–8019.

46. Y. Zhang, H. Wu, Z. Hu, J. Wang, Y. Wu, H. Yu, *Inorg. Chem. Front.*, 2022, **9**, 4075–4080.
47. B.-W. Liu, H.-Y. Zeng, X.-M. Jiang, and G.-C. Guo, *CCS Chem.*, 2021, **3**, 964–973.
48. W.-F. Chen, B.-W. Liu, S.-M. Pei, X.-M. Jiang, G.-C. Guo, *Adv. Sci.*, 2023, **10**, 2207630.
49. Z.-X. Wu, W.-F. Chen, X.-M. Jiang, B.-W. Liu, G.-C. Guo, *Chem. Mater.*, 2024, **36**, 3444–3451.
50. S.-M. Pei, B.-W. Liu, X.-M. Jiang, Y.-Q. Zou, W.-F. Chen, Q.-N. Yan, G.-C. Guo, *Chem. Mater.*, 2021, **33**, 8831–8837.
51. B.-W. Liu, S.-M. Pei, X.-M. Jiang, G.-C. Guo, *Mater. Horiz.*, 2022, **9**, 1513–1518.
52. S.-M. Pei, B.-W. Liu, W.-F. Chen, X.-M. Jiang, G.-C. Guo, *Mater. Horiz.*, 2023, **10**, 2921–2926.
53. J. Zhou, K. Hou, Y. Chu, Z. Yang, J. Li, S. Pan, *Small*, 2023, 2308806.
54. F. Wu, W.-F. Chen, Z.-X. Wu, X.-M. Jiang, B.-W. Liu, G.-C. Guo, *Sci. China. Mater.*, 2024, **67**, 2000–2007.
55. Y. Guo, W.-F. Chen, M.-X. Li, F. Wu, Q.-P. Qin, B.-W. Liu, X.-M. Jiang, G.-C. Guo, *Chem. Mater.*, 2024, **36**, 4838–4848.